Differential regulation of GUV mechanics via actin network architectures

Nadab H. Wubshet^a, Bowei Wu^b, Shravan Veerapaneni^c, Allen P. Liu^{a,d,e,f,*}

^aDepartment of Mechanical Engineering, University of Michigan, Ann Arbor, MI 48109

^bDepartment of Mathematical Sciences, University of Massachusetts Lowell, Lowell, MA 01854

^cDepartment of Mathematics, University of Michigan, Ann Arbor, MI 48109

^dDepartment of Biomedical Engineering, University of Michigan, Ann Arbor, MI 48109

^eCellular and Molecular Biology Program, University of Michigan, Ann Arbor, MI 48109

^fDepartment of Biophysics, University of Michigan, Ann Arbor, MI 48109

*Corresponding author: Allen P. Liu

Email: allenliu@umich.edu

Keywords: Actin network reconstitution; Giant vesicle electrodeformation; Numerical analysis

Abstract

Actin networks polymerize and depolymerize to construct highly organized structures, thereby, endowing the mechanical phenotypes found in a cell. It is generally believed that the amount of filamentous actin and actin network architecture determine cytoplasmic viscoelasticity of the whole cell. However, the intrinsic complexity of a cell and presence of endogenous cellular components make it difficult to study the differential roles of distinct actin networks in regulating cell mechanics. Here, we model a cell by using giant unilamellar vesicles (GUVs) encapsulating actin filaments and networks assembled by various actin crosslinker proteins. Perturbation of these cytoskeletal vesicles using AC electric fields revealed that deformability depends on actin network architecture. While actin-free vesicles exhibited large electromechanical deformations, deformations of GUVs encapsulating actin filaments were significantly dampened. The suppression of electrodeformation of actin-GUVs can be similarly recapitulated by using aqueous PEG 8000 solutions at different concentrations to modulate solution viscoelasticity. Furthermore, alpha actinin-crosslinked actin networks resulted in decreased GUV deformability in comparison to actin filament-encapsulating GUVs, and membrane-associated actin networks through the formation of dendritic actin cortex greatly dampened electrodeformation of GUVs. These results highlight the organization of actin networks regulates the mechanics of GUVs and shed insights into the origin of differential deformability of cells.

Statement of Significance

Cells differentially regulate their mechanical properties on their own accord allowing them to seamlessly execute biological tasks in a changing environment. Cellular mechanophenotype is generally attributed to the cytoskeleton, and particularly, the actin cytoskeleton, which self-assembles from actin building blocks and actin binding proteins (ABPs) into elaborate networks. Prior in vitro studies have suggested the diverse organization of cytoskeletal networks differentially endow cellular mechanics. Although bulk reconstitution studies have explored actin network phenotypes assembled by various ABPs as crosslinkers, their mechanical characterization in an isolated cell-like confinement remains largely unexplored. Here, using bottom-up reconstitution of actin networks, we demonstrate that differential cellular mechanics is mediated through assembly of distinct actin architectures.

Introduction

The cell's ability to change shape to support cellular functions such as migration and division, and its ability to resist deformation to sustain structural integrity, depends on the cytoskeleton. Among different types of cytoskeletal polymers, actin filaments assemble into various networks aided by actin binding proteins that form large-angle-crosslinks, bundles, and branches (1,2). Although the flexural rigidity of actin filaments is as much as three orders of magnitude lower compared to that of microtubules (3), assembly of actin filaments into highly organized and dynamic networks gives rise to enhanced viscoelastic property (1,4,5). As a result, actin networks endow the mechanical phenotype of cells by differentially regulating the elasticity and cytoplasmic viscosity of cells (6). Prior research have linked the mechanical property of cells to the actin network (5,7). For example, it is reported that increased deformability of ovarian cancer cells, due to their actin organization, is directly correlated to metastatic transformation (8,9). Furthermore, retraction of epithelial cells to break cell-cell junction as a result of local actin disruption is linked to extravasation of cancer cells during metastatic invasion (10,11). It is also known that cytoplasmic viscosity of red blood cells affects their dynamics inside microvasculatures (12,13). The connection between cell mechanics and cellular processes has led to substantial interest in perturbing the cytoskeleton as a means to regulate cellular processes.

Due to the simple experimental set up, many have utilized electromechanical perturbation of cells using both direct current (DC) and alternating current (AC) electric fields. Earlier studies using electroperturbation dealt with the interaction of pulsed DC electric field and cell membranes that resulted in electropermeabilization and electroporation (14). Controlled modulation of DC electric fields resulted in the formation of enlarged pores permitting the introduction of large molecules that are otherwise not permeable through cell membrane, thus giving rise to various applications including DNA transfection, drug delivery, cancer therapy (15– 17), and gene therapy (18,19). Strong AC fields, on the other hand, are known to induce cellular deformation. The semi-permeable lipid bilayer of a cell's plasma membrane can be thought of as an electrical insulator. When an electric field is applied, ions inside a cell undergo charge separation resulting in dielectrophoresis due to a non-uniform electric field (20). Depending on the electric field strength and conductivity of the suspension environment, dielectrophoretic forces result in the deformation of cells (21). Many studies have resorted to AC electrodeformation to measure apparent stiffness of red blood cells and platelets (22.23). viscoelasticity of cancer cells (24,25), and to study the effect of actin depolymerization on the relaxation of electrodeformed cells (26).

Although prior studies have revealed the mechanical properties of cells are intimately tied to their actin networks, the differential role of actin, in the form of filaments and networks, on the deformability of cells remain incompletely understood. The intrinsic complexity of cells and numerous endogenous components make it difficult to study the differential roles of actin networks as a function of actin crosslinkers (27). Giant unilamellar vesicles (GUVs) present a unique platform to model and reconstitute cellular processes in a membrane-confined environment (28). This experimental approach has been used to study the assembly of different types of actin networks (29), how actin network induces membrane remodeling (30–34), and to reveal actin binding protein competition and cooperation in actin network assembly (35,36). Others have also reconstituted a cortex-like shell in GUVs and measured their responses to mechanical compression (37).

The responses of GUVs to applied electric field have been extensively investigated (38–44). Subject to strong DC pulses, similar to cells, macropores formed in GUVs when the transmembrane potential threshold was exceeded (40). Vesicle closure after poration, curvature

relaxation and other electrical properties of GUVs have been characterized for different bilayer compositions and salt concentrations used for both the external medium and the GUV lumen (38,40,45–47). Furthermore, it has been shown that when induced by a DC pulse, GUVs with an actin cortex have suppressed membrane permeability compared to cortex-free GUVs (48), presumably due to smaller and/or less macropore formation. Similar to cells, strong AC electric fields forced spherical GUVs to assume elliptical shapes with the major axis either parallel (prolate) or perpendicular (oblate) to the electric field (49). GUVs undergo these shape transformations depending on the salt concentration ratio between the GUV lumen and the solution outside of GUVs, and electric field strength and frequency (39,49,50). AC field electrodeformation transitions have been theoretically modeled under different conditions (51–53), and experimental studies based on electrodeformation have investigated bilayer properties such as membrane bending rigidity and bilayer viscosity (40,54). Although GUV membrane properties have been well studied and characterized, how the mechanics of GUV is influenced by different actin network architectures remains incompletely understood.

Here, we investigate the effect of encapsulated actin filaments and crosslinked actin networks on the electrodeformability of GUVs in response to AC electric fields. We encapsulated actin-free buffer solution and filamentous actin inside GUVs. Subject to an AC electric field, we observed a significant difference in deformability between the two conditions. We modulated the viscosity of GUV lumen and found that the deformability of GUVs correlated with lumenal viscosity, a condition that mimics filamentous actin. Furthermore, crosslinked or membrane-cortex actin networks, at the same concentrations of F-actin, further dampened GUV electrodeformation. Overall, our results reveal that the differential mechanical properties of GUVs, and by extension to cells, can be modulated by actin network architectures.

Materials and Methods

Reagents

Purified actin was purchased (Cytoskeleton, Inc.). ATTO 488 actin was purchased from Hypermol (Germany). Actin crosslinker alpha-actinin from rabbit skeletal muscle and Arp2/3 complex from bovine brain were purchased form Cytoskeleton, Inc.. Hexa-histidine-VCA (His6-tag VCA) was purified as described previously (36). General actin buffer (G-buffer) was prepared at 10x concentration and consists of 50 mM Tris-HCL pH 8.0, and 2 mM CaCl2. Actin was diluted from a stock concentration of 10 mg/ml to a working concentration using G-buffer + 0.2 mM ATP and 0.5 mM DTT. Actin polymerization buffer (F-buffer) was prepared at 10x concentration and is composed of 500 mM KCl, 20 mM MgCl2, and 10 mM ATP. 1,2-dioleoyl-sn-glycero-3-phosphocholine (DOPC), 1,2-dioleoyl-sn-glycero-3-[(N-(5-amino-1-carboxypentyl)iminodiacetic acid)succinyl] (nickel salt) (DGS-NTA(Ni)), and cholesterol were purchased from Avanti Polar Lipids. PEG 8000 was purchased from Fisher Scientific. Density gradient medium (Optiprep) and other chemicals were purchased from Sigma Aldrich.

Electrodeformation setup

A simple homemade electroperturbation chamber was assembled to conduct GUV electrodeformation experiments. The setup is comprised of adhesive electrode tape and 3 x 1 in coverslip. Two copper tapes were used as electrodes and were attached to one face of the coverslip in a parallel manner with gaps ranging from 200-300 μ m. Sinusoidal AC electric field was applied using an Agilent 33120A (Keysight Technologies, USA) function generator between electrodes adhered to coverslip. We used a fixed length of electrode tapes, and using voltmeter (Fluke, USA), we measured potential of 6.7 V when applying 10 V peak to peak sinusoidal AC. Lower than RMS voltage measured at the electrodes end may be attributed to resistance from

adhesive and tape length. To apply identical AC field between slightly varying chambers between different devices, applied voltage was adjusted accordingly to the exact measured gap between the two electrodes such that 30 kV/m is the applied field strength between the electrodes. During electroperturbation experiments, GUVs were dispensed between the electrodes. The height of the copper tape, which is ~100 μ m, was higher than nearly all sizes of generated and analyzed GUVs, therefore yields a uniform electric field across the length of the chamber. For all experiments, duration of AC field was kept within 3-4 seconds.

GUV generation

Encapsulation of aqueous material inside GUVs was achieved using the modified cDICE method (55). As described previously (36), a 3D printed cDICE chamber is mounted onto a table top stirring motor and rotated at 1200 rpm. First, 770 µL outer aqueous glucose solution, of varying concentrations depending on osmotic condition, is dispensed into the chamber. For isoosmotic conditions, concentration of glucose is tuned such that its osmolarity matches the measured osmolarity of the inner solution, whereas for hyperosmotic conditions (flaccid GUVs), the outer glucose solution is 400 mOsm higher than inner solution. Next an adequate amount of oli/lipid mixture is dispensed into the chamber. The lipid composition used in all conditions, except for reconstituting actin cortex, is 70 mol% DOPC with the addition of 30 mol% cholesterol. During reconstitution of the actin cortex, 5 mol% DGS NTA(Ni) was added to the lipid composition while lowering cholesterol to 25 mol%. Oil is composed of 80% silicon oil and 20% mineral oil. When oil and lipid solutions are mixed, a two-phase dispersion emerges due to the emulsification of mineral oil containing lipid aggregates. Upon the addition of the lipid/oil mix to the chamber, it forms an interface saturated by lipid aggregates. Separately, 770 µL of oil/lipid mix is dispensed in to an epitube containing 20 µL of prepared inner solution (encapsulant) and pipetted up and down until the solution becomes cloudy indicating formation of lipid monolayer saturated encapsulant emulsions. Finally, the solution is transferred to the cDICE chamber. Due to centrifugal forces generated by the rotating chamber, encapsulant emulsions are shuttled through the oil/lipid mix into the outer solution. When emulsions cross the lipid saturated interface, a second layer of lipid zips the emulsions and forms GUVs suspended in the outer aqueous solution.

Inner solution preparation

Various inner solution conditions were reconstituted to conduct GUV electroperturbation experiments. Each condition contains 7.5% density gradient medium to facilitate GUV sedimentation. In viscosity contrast experiments, PEG 8000 was dissolved in DI water at specified concentration (2%, 4%, and 8% w/v). To reconstitute actin-polymerization-buffer GUVs, inner solution contained 1x F buffer and 3 mM ATP. For reconstitution of F-actin GUVs all components in the inner solution of actin-polymerization-buffer GUVs are preserved with the addition of 5.3 µM actin and 0.53 µM ATTO 488 actin. The electrical conductivity of G-buffer and F-buffer used to reconstitute globular actin and filamentous actin, respectively, was measured using a benchtop conductivity meter Orion Star A212 (Thermo Scientific, USA). Furthermore, viscosity measurements of actin and buffer solutions were conducted using Discovery HR-2 rheometer (TA Instruments, USA) at a shear rate of 100 s⁻¹ and 25 °C. To reconstitute alphaactinin-crosslink GUVs, all ingredients used to reconstitute F-actin were mixed and incubated for 15 minutes in ice. Then, 1.77 µM of alpha-actinin was added to the solution. Addition of alphaactinin, or any actin crosslinker, should be immediately followed by the last step of the cDICE GUV generation method, which is making lipid monolayer stabilized inner solution emulsions by mixing actin solution with lipid/oil mix followed by dispensing into the cDICE chamber. For reconstitution of actin cortex, the lipid composition is slightly altered by the addition of 5 mol%

DGS NTA(Ni). Similar to alpha-actinin-crosslinked actin network reconstitution, F-actin components were incubated in ice for 15 minutes. Then actin nucleation promotion factor, 0.5 μ M His₆-tagged VCA, is added followed by addition of 0.5 μ M of Arp2/3 complex. When confined by the lipid bilayer compartment, His₆-tagged VCA binds to nickel domain of DGS NTA(Ni) and activates Arp2/3 to form dendritic actin networks restricted at the lipid bilayer membrane.

Imaging

In our experiments, we used two different imaging setups: bright-field imaging equipped by a high-speed camera and fluorescence imaging using a confocal microscope. To acquire dense data points yielding contentious deformation profile of GUVs when subject to AC electric field, Olympus CKX41 (Olympus, USA) inverted microscope equipped with Phantom Miro ex1 (Phantom High Speed, USA) high-speed camera was used. Images were taken at a rate of 1200 fps using a 40x/0.55 NA objective lens and acquired using phantom camera control (PCC 1.2) software. To observe actin dynamics in response to electric field, we used an Olympus IX-81 inverted microscope equipped with a spinning disk confocal (Yokogawa CSU-X1), OBIS LS/LX lasers (Coherent, USA) and an iXON3 EMCCD camera (Andor Technology, USA). Each component was controlled by using MetaMorph (Molecular Devices, USA). Images were acquired using an oil immersion 40x/1.3 NA objective. While GUV samples were inside the electroperturbation chamber and subject to an AC electric field, ATTO 488 actin was excited using 488 nm laser at an exposure time of 170 ms, and time-lapse images were taken every 200 ms. Maximum deformation measured from confocal images were, along with bright-field images, used for statistical analysis of each GUV condition.

Statistical analysis

Using Origin software, one-way ANOVA tests were used to determine the statistical significance of major axis to minor axis ratios across different conditions. Furthermore, p values were determined using two-tailed Student's t-test. p < 0.05 is considered statistically significant. Number of vesicles measured range from 10 to 15 with at least three different devices used for a given condition.

Results

Actin network reconstitution in GUVs and electroperturbation device

To reconstitute various actin networks in cell-sized lipid vesicles, the modified continuous droplet interface crossing encapsulation (cDICE) method (55) (**Fig. 1A**) was used. In the presence of actin crosslinkers, actin networks formed rapidly and the modified cDICE method renders rapid encapsulation of actin networks to permit network assembly postencapsulation. Actin filaments, components of actin cortex, and large-angle actin crosslinker (**Fig. 1B**) were encapsulated into heterogeneously sized GUVs composed of 70 mol% DOPC and 30 mol% cholesterol. 5 mol% DGS-NTA(Ni) was added when reconstituting actin cortex. Actin cortex was assembled by activating Arp2/3 complex at the inner leaflet of bilayer membrane via constitutively active His₆-tagged VCA domain of neural Wiskott Aldrich syndrome protein (N-WASP). Crosslinked networks were formed using the large-angle actin crosslinker alpha-actinin.

A simple electroperturbation device with two parallelly aligned and spaced electrodes was assembled on a glass slide to subject GUVs to AC electric fields at 5 kHz (**Fig. 2A**, **Fig S1A,B**). Electroperturbation experiments were performed by dispensing GUVs into the device chamber (i.e. space between electrodes), then applying a sinusoidal AC wave from a function

generator. Transition of vesicles from undeformed to deformed to undeformed states following a 30 kV/m AC field at 5 kHz for a duration of 3-4 s was captured using a high-speed camera mounted on a brightfield optical microscope. This setup allowed us to analyze fast real-time GUV shape transformation at a high temporal resolution.

Actin filaments dampen electrodeformability of GUVs

First, we validated our electroperturbation setup by replicating known GUV electroperturbation responses under different ionic conditions. During AC field electroperturbation, the orientation of elliptical deformation depends on the conductivity ratio $\Lambda = \frac{\sigma_{in}}{\sigma_{ex}}$, where σ_{in} is the conductivity of inner solution and σ_{ex} is the conductivity of outer solution (50). GUVs assume a prolate shape when $\Lambda > 1$ and subjected to a low frequency field and an oblate shape when $\Lambda < 1$ and subjected to a high frequency field. By tuning NaCl concentration in the inner and outer solutions and applying 30 kV/m, GUVs transformed from spherical to prorate (**Movie S1**) and spherical to oblate (**Movie S2**) shapes for $\Lambda > 1$ with a low frequency field (1kHz) and $\Lambda < 1$ with a high frequency field (50 kHz), respectively. Prolate deformations have major axis of ellipse parallel to the field direction, whereas oblate deformations have ellipse major axis orthogonal to the electric field.

To examine the impact of actin on GUV mechanics, we next investigated GUV deformability with and without the presence of encapsulated actin filaments (Fig. 2). As a control, we encapsulated actin polymerization buffer, without the presence of actin, under isoosmotic condition. Actin polymerization buffer (hereon referred to as F-buffer) contains 1x Fbuffer, 3 mM ATP, and 7.5% density gradient medium. This reaction condition contains all the reagents that are used to reconstitute filamentous actin (F-actin) and serves as the benchmark control against actin-containing GUVs. The conductivity ratio between inner and outer solution was maintained since the salt concentrations were similar for the two conditions. Considering buffers used to reconstitute actin contain tens of mM of salt molecules, we have no reason to believe charged proteins like actin at concentrations below 10 µM will result in a significant change in conductivity. The conductivity of G-buffer and F-buffer solutions were ~1.2 and ~8.0 mS/cm, respectively (Fig. S2), but we were unable to measure the conductivity of F-actin solution due to the volume required for conductivity measurements with our setup. As expected, GUVs with F-buffer assumed prolate deformation (Fig. 2B top). To show that the electrodeformation is not due to GUV deflation, which can induce exaggerated deformability during electroperturbation, a control electroperturbation experiment was performed on flaccid GUVs (from hyper-osmotic condition) containing F-buffer (Fig. 2B bottom). This resulted in greatly increased prolate deformation of GUVs compared to their iso-osmotic counterparts. We also observed an extended delay in relaxation time for flaccid GUVs. Extended relaxation time for flaccid vesicles may be attributed to excess membrane surface area with greater membrane undulation suppressing a quick recovery. As a control, when globular actin (G-actin) is encapsulated instead, their maximum deformability is more similar to the case of F-buffer than F-actin (Fig S3).

Next, we reconstituted F-actin inside GUVs. Strikingly, when applying the same AC electric field to GUVs containing 5.3 μ M F-actin in iso-osmotic condition, deformation was significantly dampened (**Fig. 2C**, **Movie S3**). Comparing each of the above 3 conditions, the largest maximum mean deformation a/b ~ 2.42 (**Fig. 2D middle**) was attained by flaccid vesicles, followed by F-buffer GUVs at a/b ~ 1.45 (**Fig. 2D left**), and the largest deformation resistance resulted in maximum mean deformation a/b ~ 1.23 for F-actin GUVs (**Fig. 2D right**). As shown in **Figure 2E**, the average maximum deformation from a population of F-buffer GUVs was significantly larger than that of F-actin GUVs. Additionally, we encapsulated F-actin at 2.65

 μ M and 10.6 μ M (**Fig S4**) and found that GUVs were more deformable under the same electroperturbation conditions at 2.65 μ M F-actin compared to 5.3 μ M and 10.6 μ M although differences between 5.3 and 10.6 μ M F-actin conditions were not significant (**Fig S4B**). In our analysis, we selected GUVs of size range 10-30 μ m that are representative of the GUV population generated using the modified cDICE method, and found no size dependent correlation between GUV size and GUV deformability (**Fig. S5**).

Considering known GUV parameters and their respective electroperturbation responses, our observation was not readily explained. In each of the above cases, there were no observed instances of electroporation to affect deformation behavior which can commonly be identified by loss of volume, loss of contrast, or by micron-sized membrane ruptures that can be observed at high magnifications. The conductivity ratio, lipid bilayer composition, and osmolarity between F-buffer GUVs and F-actin GUVs were the same. Thus, the distinct deformability behaviors can only be attributed to the material property of the GUV lumen. As a viscoelastic material, previous works have shown that a F-actin solution has an increased viscoelasticity compared to aqueous buffer solutions similar to our polymerization buffer (~1 mPa.s) and the viscosity increases further with increasing actin concentration (56). We confirmed these by measuring the viscosity of F-buffer (1.33 mPa.s) and 5.3 μ M F-actin (2.21 mPa.s) solutions with added 7.5% density gradient medium (**Fig. S6**). Thus, we hypothesized that the dampened GUV deformation was due to changes in GUV lumenal viscoelasticity.

Changes in lumenal viscosity determines the electrodeformability of GUVs

To investigate the role of change in viscoelastic property GUV lumen on electrodeformability, we encapsulated poly(ethylene glycol) (PEG) polymer solutions, which are known to be viscoelastic (57,58). PEG 8000 solutions with concentrations ranging from 2-8% w/v were encapsulated inside GUVs. Osmolarity of the outer solution was matched to the measured osmolarity of each aqueous PEG 8000 solutions in order to maintain iso-osmotic conditions. When GUVs containing 2% PEG 8000 were subjected to 30 kV/m AC field at 5 kHz for a duration of 3-4 seconds (**Fig. 3A top, Movie S4**), the maximum mean deformation was measured at a/b ~ 1.3 (**Fig. 3B left**). At 4% PEG 8000, the maximum mean deformation reduced to a/b ~ 1.14 (**Fig. 3A middle, Fig. 3B right, Movie S5**). In GUVs with 8% PEG 8000, no measurable GUV deformation was observed (**Fig. 3A bottom, Movie S6**), and thus there is no deformation profile included for the 8% PEG condition. Our results clearly demonstrated dampening of GUV deformation with increasing lumenal viscosity (**Fig. 3C**), consistent with our initial hypothesis that dampened deformation in F-actin GUVs is related altered lumenal viscosity.

The degree of deformability of 5.3 µM F-actin GUVs falls between deformability of GUVs encapsulating 2% PEG and 4% PEG solutions, and directly corresponds to the measured viscosity of F-actin solution at this concentration (2.21 mPa.s) that is in between the viscosity of 2 and 4% PEG solutions. Although these observations may be intuitive and in alignment with our initial hypothesis, to our knowledge, there are no prior studies that exploited cell-mimicking confinements like GUVs to investigate the effect of lumenal material property on their electrodeformability. Thus, here we illustrate a mechanism for cells to maintain structural integrity by only modifying viscosity without necessitating crosslinking of cytoskeleton using additional actin binding proteins.

In silico investigation on the role viscosity contrast on GUV electrodeformability

We developed a computational method to further investigate the role of viscosity contrast (detailed in SI). Numerical experiments are set up by placing the GUV in an AC field $\mathbf{E}_{\infty}(t)$ with magnitude E_0 , such that

$$\boldsymbol{E}_{\infty}(t) = E_0 \sin(2\pi\omega t)\,\widehat{\boldsymbol{x}}$$

where ω is the AC field frequency. Using the GUV radius a as the characteristic length scale and the membrane charging time $t_m = aC_m/\sigma_{\rm ex}$ as the characteristic time scale, we define the following dimensionless parameters:

viscosity ratio: $\eta = \mu_{in}/\mu_{ex},$ conductivity ratio: $\Lambda = \sigma_{in}/\sigma_{ex},$ electric field strength: $\beta = \epsilon_{ex} E_0^2 t_m/\mu,$ AC field frequency $\Omega = \omega t_m.$

An AC field of frequency $\Omega=0.5$ and strength $\beta=10$ is applied at t=0 and we measure the aspect ratio a/b of the GUV over time. We observe that, for a fixed conductivity ratio Λ , the prolate deformation of the GUV is delayed as the viscosity contrast η is increased (**Fig. 4A**). Additional experimental results, shown in **Figure S7**, indicate that fixing the conductivity ratio Λ of 2% (**Fig. S7A**) and 4% PEG 8000 (**Fig. S7B**) concentrations to 0.9, by addition of 7.5 mM NaCl to 4% PEG 8000 inner solution, preserved deformation dampening as a result of increasing η (**Fig. S7C,D,E**). For a fixed viscosity contrast, the prolate deformation happens only when the conductivity ratio Λ is large enough (**Fig. 4B**). Consequently, dampening of the prolate deformation is observed as a combined effect of increasing η and decreasing Λ (**Fig. 4C**), which is consistent with the experimental results using PEG 8000 solutions with increasing concentrations (**Fig. 3**).

One advantage of the numerical approach presented in this section is its ability to collect a variety of quantities of interest that will be useful for further investigations. For example, we have shown in Figure 4D the contour plots of the electric potential around the vesicle that corresponds to different stages of the deformation, where it is clear that when the vesicle is being stretched during the transitioning stage, the electric field strength is almost uniformly zero inside the GUV. Transient square-like shaped deformation is a result of our simulation assuming impermeable membrane.

Structurally distinct actin networks differentially regulate GUV mechanics.

Mechanical features and responses of actin networks are governed by actin binding proteins and particularly actin crosslinkers. These crosslinkers not only assemble phenotypically distinct networks but also spatially organize actin networks allowing the cell to have variable mechanics across the cell volume. How might structurally distinct actin networks in a cellmimicking confinement determine mechanical behavior? Here, we examined GUVs with Arp2/3branched dendritic actin cortex (actin-cortex GUVs) or networks made with a large-angle actin crosslinker alpha-actinin (alpha-actinin-crosslink GUVs). Membrane-bound dendritic actin cortex was achieved by activation of Arp2/3 complex using membrane-associated nucleation promotion factor (His6-tagged VCA) on DGS NTA(Ni)-containing membrane. Encapsulating actin with His6-tagged VCA-activated Arp2/3 complex generated uniform actin-cortex GUVs with a high efficiency (Fig. 5A right, 5C top). Absence of DGS NTA(Ni) prevents the localization of His₆-tagged VCA to the membrane consequently inhibiting the reconstitution of actin cortex (Fig. **5A. B**). On the other hand, alpha-actinin addition led to a range of actin network morphologies. including rings, asters and random networks (Fig. 5C bottom). Although reconstitution of various actin networks is well established to study crosslinkers and network phenotypes (35,36,59,60), little is known about how these actin crosslinkers differentially regulate GUV deformability.

We followed the same electroperturbation procedure employed in previous experiments and subjected actin cortex GUVs to an AC field. Electrodeformability of actin-cortex GUVs was

greatly dampened and hardly visible to the naked eye (**Fig. 5D**). Under the same condition, GUVs with alpha-actinin-crosslinked networks were more deformed compared to actin-cortex GUVs (**Fig. 5E**). Electrodeformation was dampened to the largest extent by actin-cortex GUVs with a max mean deformation a/b ~ 1.07 (**Fig. 5F top**), and alpha-actinin-crosslink GUVs had a max mean deformation of a/b ~ 1.15 (**Fig. 5F bottom**). Compared to the F-actin GUVs, both actin-cortex and alpha-actinin-crosslink GUVs had reduced deformability, with extreme dampening in actin-cortex GUVs (**Fig. 5G**). Looking closely at the deformation profile of actin-cortex GUVs, strangely, as shown in Figure 5D top, deformation was not sustained over the duration of AC field application, but rather GUVs started to recover immediately after reaching max deformation. Similar profile was not observed for alpha-actinin-crosslinked GUVs as they maintained deformation throughout the duration of applied AC field.

VCA is an acidic protein and its binding to the membrane may alter the dielectric property of GUV thereby its deformation under the electric field. When we included VCA and in the absence of Arp2/3 complex, we did not observe dampening of deformation (**Fig 6A**), indicating that the actin cortex itself was likely the major contributor to the observed deformation dampening. Consistent with this, leaving out NTA(Ni) lipid altogether also did not lead to a large deformation dampening (**Fig 6A**). We have presented these results comparing them to actincortex and F-actin GUVs (**Fig 6B**). Furthermore, we modulated the concentrations of NTA(Ni) and reduced NTA(Ni) lipids from 5% to 2.5%, we found a notable recovery of GUV deformability (**Fig. 6C**), yet with significantly enhanced deformation dampening compared to alpha-actinin-crosslink GUVs (**Fig. 6D**). Presumably, controlling the density of actin cortex effectively tuned GUV deformability.

These results demonstrated differential mechanical properties of various isolated actin networks in a cell-like confinement. The mechanism by which actin networks achieve such mechanical variation is still open to investigation.

Discussion

In this work, we examined how the structural arrangement of lumenal contents determines electrodeformability of cell-mimicking GUVs subjected to an AC electric field. This mechanism is distinct from conditions that are known to impact the degree of electrodeformation which include conductivity contrast, osmotic contrast, lipid bilayer composition, lipid bilayer viscosity, and electric field intensity (41,50,51,54). In contrast, our results show that deformability of GUVs encapsulating actin filaments is suppressed compared to actin-free GUVs. We demonstrated the deformation dampening of F-actin GUVs is likely manifested as increasing viscosity of the GUV lumen. Motivated by differential mechanics found in a cell, we further examined how actin cortex and crosslinked actin networks govern GUV electrodeformation. Evident from dampened deformation, our results illustrate differences in GUV deformability between different actin architectures, when they have identical total actin concentrations

The mechanism by which deformability of GUVs is dampened as a function of increasing viscosity is not apparently clear. To gain some insights, it is necessary to consider the inherent property of actin and PEG as polymer chains. Polymer chains such as actin and PEG, depending on the average polymer length and dispersity are known to entangle at random (61–63). Thus, one possible physical model that can be entertained as a plausible mechanism is from disordered polymer chain entanglement altering the strain-dependent (elastic) property of the GUV-encapsulant. Prior works have shown that there exists a relationship between polydispersity of polymer chains and their respective elasticity (64), thereby resulting in a change in permanent compressibility. Polymer chain entanglements constrain transient deformability of a viscoelastic composite such as the GUV-encapsulant composite by physically

creating a barrier where entanglement networks are unable to relax/separate. Thus, it is within reason to consider the theory that an increase in viscosity in response to increasing the concentration of polymer chain is simultaneously changing the elastic property of actin encapsulating GUVs. In the future, other physical models and theories can be investigated as potential explanations for the dampening of deformation as a function of increasing viscosity of the GUV lumen. We acknowledge that cell cytoplasm is known to be highly viscous due to the high protein contents that is not just attributed by actin filaments. While our data suggests viscosity could play a role, we believe the architecture (i.e., how they are organized and where) of the actin networks has a more dominant role here.

As revealed by our findings, actin-cortex GUVs have greater deformation resistance compared to GUVs with alpha-actinin-crosslinked networks. Prior findings by Wagner et al. show that actin crosslinkers increase viscosity of actin in bulk solutions (56). However, the structure and spatial scale of actin networks formed in bulk solutions are diametrically different from those assembled in a cell-like confinement. Thus, it would be premature to attribute our finding that actin crosslinkers differentially regulate GUV electrodeformability to simply viscosity difference. During electrodeformation, GUVs undergo two distinct deformation regimes namely entropic and elastic regimes (43). The extent of the deformation in the entropic regime is dependent on the degree of thermal undulations in the bilayer which varies depending on the lipid composition and osmotic contrast, whereas the elastic regime is dictated by field intensity and bilayer stretchability at the molecular level. These deformation regimes may potentially be altered as a result of the material property of the lumen and its interaction with the lipid bilayer membrane. Thus, it is important to consider mechanisms of how different actin networks may affect these deformation regimes beyond changes in lumenal viscosity. In this context, it will be interesting to study the effect of actin network on deswelled GUVs and how actin networks impact deswelled GUVs' deformation.

It is well established that the actin cortex regulates membrane rigidity (65,66). When thin actin-cortex shells were reconstituted in GUVs and subjected to hydrodynamic tube pulling, it was shown that the membrane tube length was reduced for thin actin shell GUVs (67). Considering this prior finding, it is possible that the mechanism of electrodeformability suppression by actin cortex is due to changes in membrane rigidity that restricts membrane undulation in the entropic regime of deformation, and thereby restricting lipid mobility, consequently reducing bilayer stretching, in the elastic regime of electrodeformation. More likely though is that the elasticity of the cortex may contribute to the increased deformability resistance of actin-cortex GUVs. For alpha-actinin-crosslink GUVs, a different mechanism may be plausible to account for their suppressed electrodeformability. When F-actin GUVs are subject to an electric field, due to the scale of individual filaments with respect to GUV size and field pressure, actin filaments are unable to individually resist deformation, akin to sand grains in quicksand, and unable to undergo individual strain. However alpha-actinin assembles complex actin scaffolds that can reinforce the GUV, like a truss system, to resist field forces. Further investigation could possibly shed more light on the relationship between crosslink/bundle rigidity and electrodeformability and a more systematic study to titrate concentrations of crosslinkers will be informative.

For the numerical simulation of the electrodeformation of GUVs, the leaky-dielectric model is used, which characterizes some key physical and mechanical properties of GUVs, including conductivity contrast, membrane rigidity, and lumenal viscosity. Our numerical simulations provide additional supporting evidence, independent of experiments, that GUVs of increased lumenal viscosity experience greater deformation resistance. An important advantage of numerical simulation is its ability to collect various quantities of interest at ease, such as electric potential and velocity fields, offering more detailed characterizations of GUV

electrodeformation. However, there are limitations to the current mathematical model. Firstly, due to its simplifying assumptions on the membrane structure, this model is incapable of capturing phenomena such as electropermeabilization and electroporation that occur under a strong electric field. Thus, our model restricts the membrane to an inextensible and intact boundary, which also explains why vesicles appear non-spherical before application of electric field. Secondly, the current model does not account for the cytoskeleton structures in GUVs, which will be important for further investigating the effect of different actin networks as integral structural components on the electrodeformability of GUVs. We think that this also explains the mismatch between our experimental and simulated results. Limitations to simulate change in the elastic behavior of entangled actin could possibly be why we fail to observe deformation dampening at steady state. To resolve these limitations in the future, more sophisticated mathematical models need to be developed.

There are many fascinating mechanobiological inquiries that can be pursued using cytoskeletal GUVs. The cell is a very dynamic and structurally and functionally complex system with many proteins involved in a single function. The GUV furnishes a cell-like confinement system that is suitable for systematic construction of complex cellular functions module by module. Using our findings as a steppingstone, we anticipate future interest in examining the role of various other types of actin networks, and co-assembled networks of actin, intermediate filaments, and microtubules, in determining mechanophenotypes. The emergent mechanics of cytoskeleton is an underexplored area of cytoskeleton and membrane research. Our work provides a starting point to examine a myriad of other actin crosslinkers and their mechanical contribution to cell mechanical properties. Such efforts will help uncover deep insights into cell mechanics from the bottom up.

Author Contributions: N.H.W. and A.P.L. designed research. N.H.W., B.W. and S.V. performed research. B.W. and S.V. contributed analytic tools. N.H.W. analyzed data. N.H.W., B.W., S.V., and A.P.L. wrote the paper.

Declaration of Interests

The authors declare no competing interests.

Acknowledgments

We thank Yashar Bashirzadeh for helpful discussion. We thank Professor Mark Burns and Anna Nelson for kindly letting us use their conductivity meter. We thank UM Battery Lab and Eleni Temeche for assisting us with viscosity measurements. The work is supported by the National Science Foundation (CBET-1844132). N.H.W. was supported by NIH's Microfluidics in the Biomedical Sciences Training Program (NIH NIBIB T32 EB005582). S.V. acknowledges support from National Science Foundation (DMS-2012424). A.P.L. acknowledges support from National Institutes of Health (R01 EB030031-01) and National Science Foundation (EF1935265 and MCB220136).

References

- 1. Tseng Y, Kole TP, Lee JSH, Fedorov E, Almo SC, Schafer BW, et al. How actin crosslinking and bundling proteins cooperate to generate an enhanced cell mechanical response. Biochem Biophys Res Commun. 2005;334(1):183–92.
- 2. Lieleg O, Claessens MMAE, Bausch AR. Structure and dynamics of cross-linked actin networks. Soft Matter. 2010;6(2):218–25.
- 3. Gittes F, Mickey B, Nettleton J, Howard J. Flexural rigidity of microtubules and actin filaments measured from thermal fluctuations in shape. J Cell Biol. 1993;120(4):923–34.
- 4. Gardel ML, Shin JH, MacKintosh FC, Mahadevan L, Matsudaira P, Weitz DA. Elastic behavior of cross-linked and bundled actin networks. Science (80-). 2004;304(5675):1301–5.
- 5. Gardel ML, Nakamura F, Hartwig J, Crocker JC, Stossel TP, Weitz DA. Stress-dependent elasticity of composite actin networks as a model for cell behavior. Phys Rev Lett. 2006;96(8):88102.
- 6. Stossel TP. Contribution of actin to the structure of the cytoplasmic matrix. J Cell Biol. 1984;99(1):15s-21s.
- 7. Schaefer A, Te Riet J, Ritz K, Hoogenboezem M, Anthony EC, Mul FPJ, et al. Actin-binding proteins differentially regulate endothelial cell stiffness, ICAM-1 function and neutrophil transmigration. J Cell Sci. 2014;127(20):4470–82.
- 8. Ketene AN, Schmelz EM, Roberts PC, Agah M. The effects of cancer progression on the viscoelasticity of ovarian cell cytoskeleton structures. Nanomedicine Nanotechnology, Biol Med. 2012;8(1):93–102.
- 9. Hu J, Zhou Y, Obayemi JD, Du J, Soboyejo WO. An investigation of the viscoelastic properties and the actin cytoskeletal structure of triple negative breast cancer cells. J Mech Behav Biomed Mater. 2018;86:1–13.
- 10. Kumar S, Weaver VM. Mechanics, malignancy, and metastasis: the force journey of a tumor cell. Cancer Metastasis Rev. 2009;28(1):113–27.
- 11. Miles FL, Pruitt FL, van Golen KL, Cooper CR. Stepping out of the flow: capillary extravasation in cancer metastasis. Clin Exp Metastasis. 2008;25(4):305–24.
- 12. Gokhin DS, Nowak RB, Khoory JA, Piedra A de la, Ghiran IC, Fowler VM. Dynamic actin filaments control the mechanical behavior of the human red blood cell membrane. Mol Biol Cell. 2015;26(9):1699–710.
- 13. Qiang Y, Liu J, Du E. Dielectrophoresis testing of nonlinear viscoelastic behaviors of human red blood cells. Micromachines. 2018;9(1):21.

- 14. Tekle E, Astumian RD, Chock PB. Selective and asymmetric molecular transport across electroporated cell membranes. Proc Natl Acad Sci. 1994;91(24):11512–6.
- 15. Nuccitelli R, Pliquett U, Chen X, Ford W, Swanson RJ, Beebe SJ, et al. Nanosecond pulsed electric fields cause melanomas to self-destruct. Biochem Biophys Res Commun. 2006;343(2):351–60.
- 16. Gothelf A, Mir LM, Gehl J. Electrochemotherapy: results of cancer treatment using enhanced delivery of bleomycin by electroporation. Cancer Treat Rev. 2003;29(5):371–87.
- 17. Heller R, Gilbert R, Jaroszeski MJ. Clinical applications of electrochemotherapy. Adv Drug Deliv Rev. 1999;35(1):119–29.
- 18. Golzio M, Teissié J, Rols M-P. Direct visualization at the single-cell level of electrically mediated gene delivery. Proc Natl Acad Sci. 2002;99(3):1292–7.
- 19. Heller LC, Heller R. In vivo electroporation for gene therapy. Hum Gene Ther. 2006;17(9):890–7.
- 20. Grosse C, Schwan HP. Cellular membrane potentials induced by alternating fields. Biophys J. 1992;63(6):1632–42.
- 21. Du E, Dao M, Suresh S. Quantitative biomechanics of healthy and diseased human red blood cells using dielectrophoresis in a microfluidic system. Extrem Mech Lett. 2014;1:35–41.
- 22. Leung SL, Lu Y, Bluestein D, Slepian MJ. Dielectrophoresis-mediated electrodeformation as a means of determining individual platelet stiffness. Ann Biomed Eng. 2016;44(4):903–13.
- 23. Gass G V, Chernomordik L V, Margolis LB. Local deformation of human red blood cells in high frequency electric field. Biochim Biophys Acta (BBA)-Molecular Cell Res. 1991;1093(2–3):162–7.
- 24. Teng Y, Pang M, Huang J, Xiong C. Mechanical characterization of cancer cells during TGF-β1-induced epithelial-mesenchymal transition using an electrodeformation-based microchip. Sensors Actuators B Chem. 2017;240:158–67.
- 25. Teng Y, Zhu K, Xiong C, Huang J. Electrodeformation-based biomechanical chip for quantifying global viscoelasticity of cancer cells regulated by cell cycle. Anal Chem. 2018;90(14):8370–8.
- 26. Wong PK, Tan W, Ho C-M. Cell relaxation after electrodeformation: effect of latrunculin A on cytoskeletal actin. J Biomech. 2005;38(3):529–35.
- 27. Bashirzadeh Y, Liu AP. Encapsulation of the cytoskeleton: towards mimicking the mechanics of a cell. Soft Matter. 2019;15(42):8425–36.
- 28. Litschel T, Schwille P. Protein reconstitution inside giant unilamellar vesicles. Annu Rev

- Biophys. 2021;50:525-48.
- 29. Merkle D, Kahya N, Schwille P. Reconstitution and anchoring of cytoskeleton inside giant unilamellar vesicles. ChemBioChem. 2008;9(16):2673–81.
- 30. Bashirzadeh Y, Wubshet NH, Liu AP. Confinement Geometry Tunes Fascin-Actin Bundle Structures and Consequently the Shape of a Lipid Bilayer Vesicle. Front Mol Biosci. 2020;7.
- 31. Litschel T, Kelley CF, Holz D, Koudehi MA, Vogel SK, Burbaum L, et al. Reconstitution of contractile actomyosin rings in vesicles. Nat Commun. 2021;12(1):1–10.
- 32. Liu AP, Richmond DL, Maibaum L, Pronk S, Geissler PL, Fletcher DA. Membrane-induced bundling of actin filaments. Nat Phys. 2008;4(10):789–93.
- 33. Maan R, Loiseau E, Bausch AR. Adhesion of active cytoskeletal vesicles. Biophys J. 2018;115(12):2395–402.
- 34. Bashirzadeh Y, Moghimianavval H, Liu AP. Encapsulated actomyosin patterns drive cell-like membrane shape changes. Iscience. 2022;25(5):104236.
- 35. Bashirzadeh Y, Redford SA, Lorpaiboon C, Groaz A, Litschel T, Schwille P, et al. Actin crosslinker competition and sorting drive emergent GUV size-dependent actin network architecture. Commun Biol [Internet]. 2021 Apr 21 [cited 2021 Sep 12];2020.10.03.322354. Available from: https://www.biorxiv.org/content/10.1101/2020.10.03.322354v3
- 36. Wubshet NH, Bashirzadeh Y, Liu AP. Fascin-induced actin protrusions are suppressed by dendritic networks in GUVs. Mol Biol Cell. 2021;mbc-E21.
- 37. Schäfer E, Kliesch T-T, Janshoff A. Mechanical properties of giant liposomes compressed between two parallel plates: impact of artificial actin shells. Langmuir. 2013;29(33):10463–74.
- 38. Teissie J, Tsong TY. Electric field induced transient pores in phospholipid bilayer vesicles. Biochemistry. 1981;20(6):1548–54.
- 39. Aranda S, Riske KA, Lipowsky R, Dimova R. Morphological transitions of vesicles induced by alternating electric fields. Biophys J. 2008;95(2):L19–21.
- 40. Riske KA, Dimova R. Electro-deformation and poration of giant vesicles viewed with high temporal resolution. Biophys J. 2005;88(2):1143–55.
- 41. Faizi HA, Dimova R, Vlahovska PM. Electromechanical characterization of biomimetic membranes using electrodeformation of vesicles. Electrophoresis. 2021;42(20).
- 42. Riske KA, Dimova R. Electric pulses induce cylindrical deformations on giant vesicles in salt solutions. Biophys J. 2006;91(5):1778–86.
- 43. Yu M, Lira RB, Riske KA, Dimova R, Lin H. Ellipsoidal relaxation of deformed vesicles.

- Phys Rev Lett. 2015;115(12):128303.
- 44. Vlahovska PM. Voltage-morphology coupling in biomimetic membranes: dynamics of giant vesicles in applied electric fields. Soft Matter. 2015;11(37):7232–6.
- 45. Riske KA, Knorr RL, Dimova R. Bursting of charged multicomponent vesicles subjected to electric pulses. Soft Matter. 2009;5(10):1983–6.
- 46. Mauroy C, Portet T, Winterhalder M, Bellard E, Blache M-C, Teissié J, et al. Giant lipid vesicles under electric field pulses assessed by non invasive imaging. Bioelectrochemistry. 2012;87:253–9.
- 47. Knorr RL, Staykova M, Gracia RS, Dimova R. Wrinkling and electroporation of giant vesicles in the gel phase. Soft Matter. 2010;6(9):1990–6.
- 48. Perrier DL, Vahid A, Kathavi V, Stam L, Rems L, Mulla Y, et al. Response of an actin network in vesicles under electric pulses. Sci Rep. 2019;9(1):1–11.
- 49. Dimova R, Bezlyepkina N, Jordö MD, Knorr RL, Riske KA, Staykova M, et al. Vesicles in electric fields: Some novel aspects of membrane behavior. Soft Matter. 2009;5(17):3201–12.
- 50. Dimova R, Riske KA, Aranda S, Bezlyepkina N, Knorr RL, Lipowsky R. Giant vesicles in electric fields. Soft Matter. 2007;3(7):817–27.
- 51. Vlahovska PM, Gracià RS, Aranda-Espinoza S, Dimova R. Electrohydrodynamic model of vesicle deformation in alternating electric fields. Biophys J. 2009;96(12):4789–803.
- 52. Nganguia H, Young Y-N. Equilibrium electrodeformation of a spheroidal vesicle in an ac electric field. Phys Rev E. 2013;88(5):52718.
- 53. Wu B, Veerapaneni S. Electrohydrodynamics of deflated vesicles: budding, rheology and pairwise interactions. J Fluid Mech. 2019;867:334–47.
- 54. Gracia RS, Bezlyepkina N, Knorr RL, Lipowsky R, Dimova R. Effect of cholesterol on the rigidity of saturated and unsaturated membranes: fluctuation and electrodeformation analysis of giant vesicles. Soft Matter. 2010;6(7):1472–82.
- 55. Bashirzadeh Y, Wubshet N, Litschel T, Schwille P, Liu AP. Rapid Encapsulation of Reconstituted Cytoskeleton inside Giant Unilamellar Vesicles. J Vis Exp Jove. 2021;(177).
- 56. Wagner O, Zinke J, Dancker P, Grill W, Bereiter-Hahn J. Viscoelastic properties of f-actin, microtubules, f-actin/α-actinin, and f-actin/hexokinase determined in microliter volumes with a novel nondestructive method. Biophys J. 1999;76(5):2784–96.
- 57. Wu X, Zhao Z, Kang Y, Ji X, Liu Y. Viscoelasticity of poly (ethylene glycol) in aqueous solutions of potassium sulfate: a comparison of quartz crystal microbalance with conventional methods. Polym J. 2019;51(5):471–80.

- 58. Zhao Z, Ji X, Dimova R, Lipowsky R, Liu Y. Viscoelasticity of poly (ethylene glycol) solutions on supported lipid bilayers via quartz crystal microbalance with dissipation. Macromolecules. 2015;48(6):1824–31.
- 59. Suarez C, Carroll RT, Burke TA, Christensen JR, Bestul AJ, Sees JA, et al. Profilin regulates F-actin network homeostasis by favoring formin over Arp2/3 complex. Dev Cell. 2015;32(1):43–53.
- 60. Burke TA, Christensen JR, Barone E, Suarez C, Sirotkin V, Kovar DR. Homeostatic actin cytoskeleton networks are regulated by assembly factor competition for monomers. Curr Biol. 2014;24(5):579–85.
- 61. Hinner B, Tempel M, Sackmann E, Kroy K, Frey E. Entanglement, elasticity, and viscous relaxation of actin solutions. Phys Rev Lett. 1998;81(12):2614.
- 62. Falzone TT, Blair S, Robertson-Anderson RM. Entangled F-actin displays a unique crossover to microscale nonlinearity dominated by entanglement segment dynamics. Soft Matter. 2015;11(22):4418–23.
- 63. McNamee CE, Yamamoto S, Higashitani K. Effect of the physicochemical properties of poly (ethylene glycol) brushes on their binding to cells. Biophys J. 2007;93(1):324–34.
- 64. Sorichetti V, Ninarello A, Ruiz-Franco JM, Hugouvieux V, Kob W, Zaccarelli E, et al. Effect of chain polydispersity on the elasticity of disordered polymer networks. Macromolecules. 2021;54(8):3769–79.
- 65. Chugh P, Clark AG, Smith MB, Cassani DAD, Dierkes K, Ragab A, et al. Actin cortex architecture regulates cell surface tension. Nat Cell Biol. 2017;19(6):689–97.
- 66. Gilden J, Krummel MF. Control of cortical rigidity by the cytoskeleton: emerging roles for septins. Cytoskeleton. 2010;67(8):477–86.
- 67. Guevorkian K, Manzi J, Pontani LL, Brochard-Wyart F, Sykes C. Mechanics of Biomimetic Liposomes Encapsulating an Actin Shell. Biophys J. 2015;109(12):2471–9.

Figures

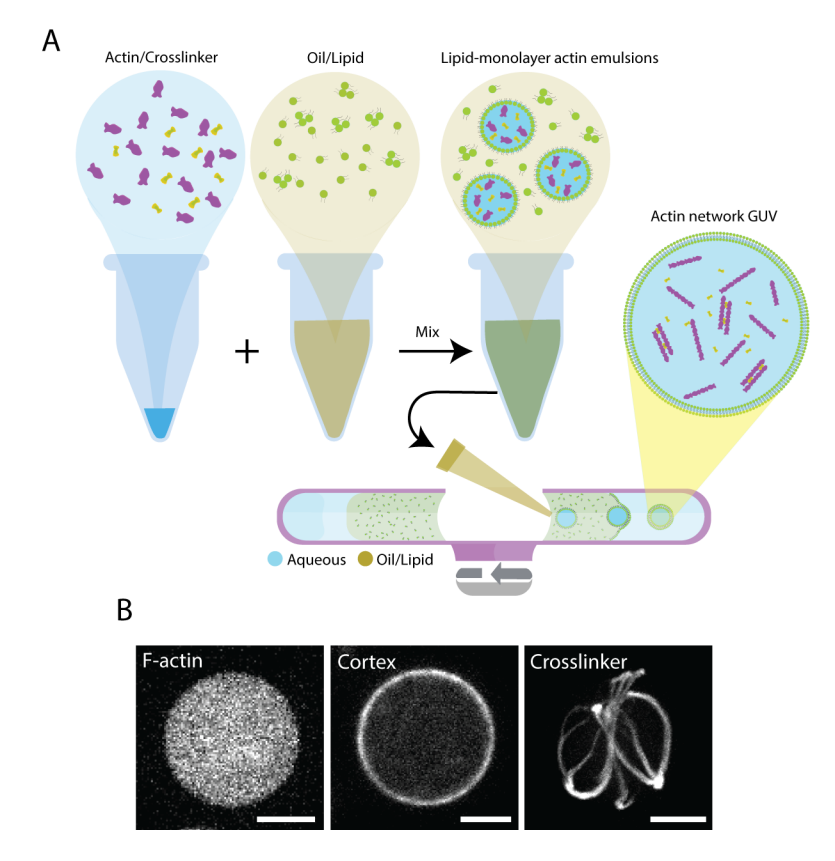


Figure 1. Reconstitution of different actin networks inside GUVs (A) Schematic of the modified cDICE method. Purple shapes represent actin monomers. Green shapes represent lipids. Yellow shapes, shown in actin/crosslinker solution schematic, represent an arbitrary actin crosslinker. (B) Representative images of actin network GUVs. (Left) Representative confocal image of encapsulated F-actin inside GUVs. (Middle) Arp2/3-complex assembled an actin cortex and associated to GUV lipid bilayer membrane. (Right) Aster-like actin network assembled by alpha-actinin encapsulated inside a GUV. Actin is labeled with ATTO 488 actin in all images. Scale bars, $10~\mu m$.

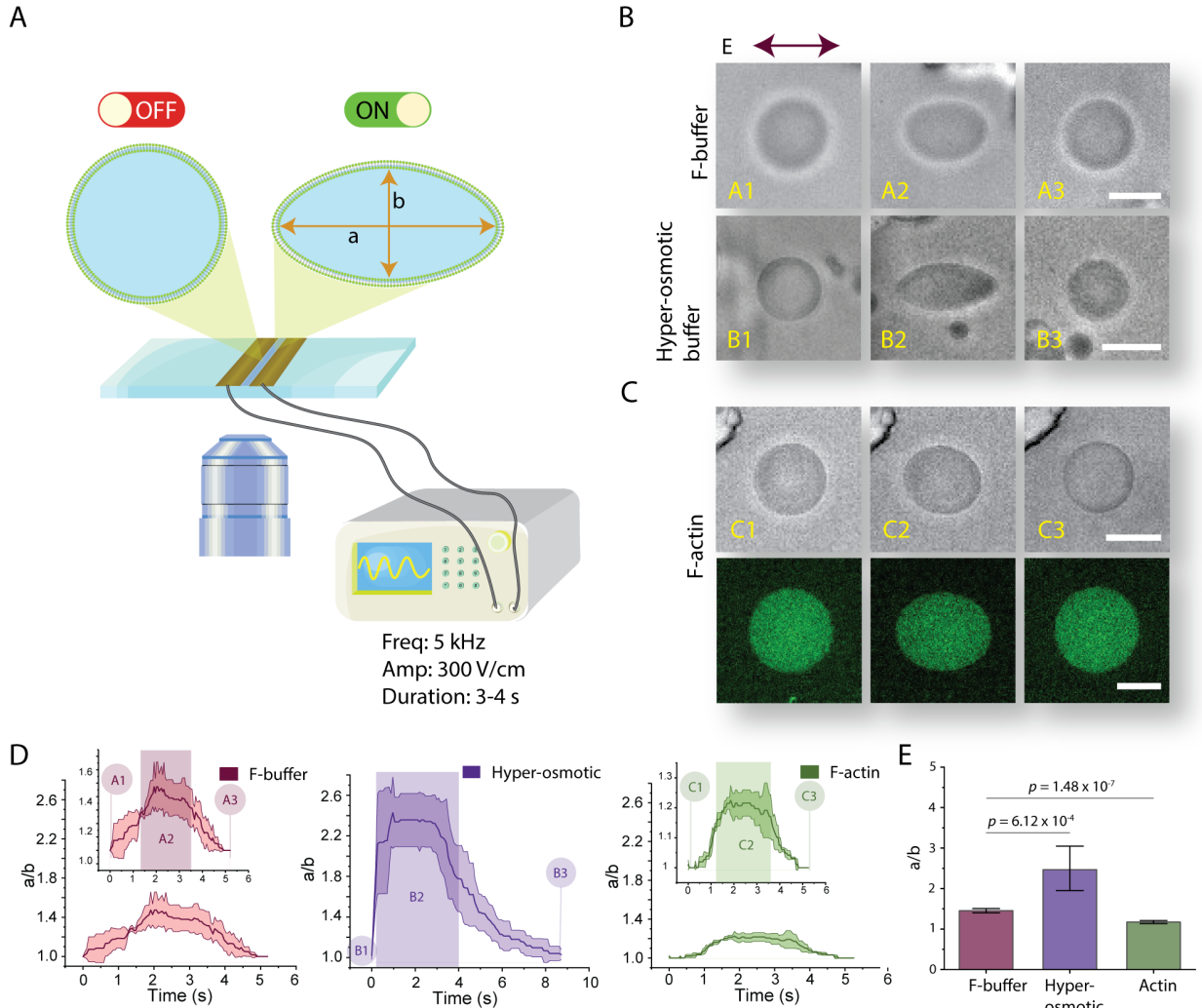


Figure 2. Lumenal content of GUVs alters deformation profile when GUVs are subjected to electroperturbation. (A) Schematic of the electrodeformation setup mounted on an inverted microscope. A function generator is operated at 30 kV/m at 5 kHz and a sinusoidal wave was applied for a duration of 3-4 seconds. Schematic shows electrodes adhered onto a coverslip. GUVs transform from a spherical shape to an ellipse when the electric field is applied. (B) GUV deformation is dependent on osmolarity difference between inner and outer solutions. (Top) Brightfield images of electric field-induced shape transformation of actin-polymerization-buffer GUVs. (A1) GUV at an undeformed state prior to AC field application; (A2) Steady-state deformation of GUVs during electoperturbation; (A3) actin-polymerization-buffer GUV post electrodeformation recovery. (B1, B2, B3) Electrodeformation of actin-polymerization-buffer GUV in a hyper-osmotic condition (flaccid GUV). (B2) shows exaggerated prolate deformation with pointed ends. (C) Electrodeformation of a F-actin GUV. (C2) shows visually apparent dampened deformation compared to A2 and B2. (C bottom) Representative fluorescence image of F-actin GUV labeled with ATTO 488 actin. (D) Deformation profile of GUV conditions in B and C for F-buffer, hyper-osmotic buffer, and F-actin conditions, as indicated. Labels (A1, A2, and A3...etc) correspond to GUV transformation stages during electroperturbation. Shaded rectangular box denotes approximate duration of electric field application. Shaded areas in the traces in each of the plots indicate ± SD, n = 3. (E) Comparison and statistical analysis of

maximum GUV deformation of each GUV condition as indicated. Data represent mean maximum deformation and error bars denote \pm SE. N_{buffer} = 11, N_{hyper} = 14, and N_{actin} = 12. Scale bars, 10 μ m.

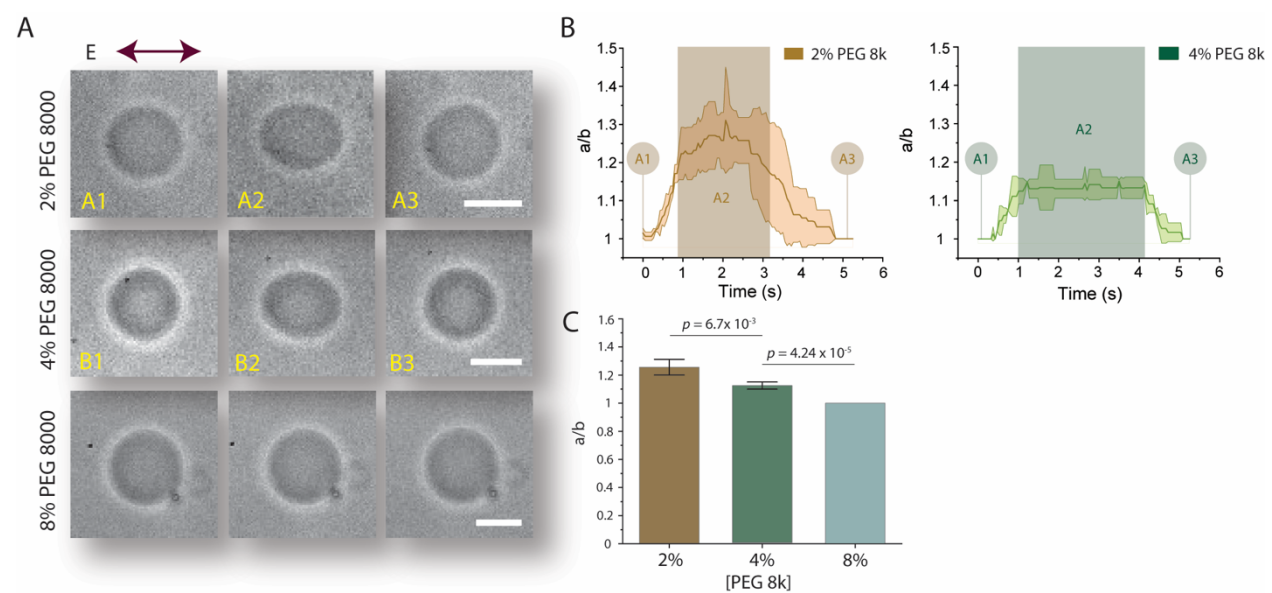


Figure 3. Relationship between viscosity contrast and electrodeformability of GUVs. Different PEG 8000 concentrations were encapsulated inside GUVs to vary viscosity contrast between GUV lumen and outer solution. (A) Brightfield images showing PEG 8000 GUV shape transitions from undeformed to elliptically deformed to spherical recovery. (Top) Electroperturbation of 2% w/v PEG 8000 GUV. (A1) A PEG 8000 GUV at an undeformed state prior to AC field application. (A2) Steady-state deformation of GUVs during electoperturbation. (A3) GUV post electrodeformation recovery to assume spherical shape. (B1-B3) 4% w/v PEG 8000 GUV electrodeformation. (Bottom) Electroperturbation of 8% w/v PEG 8000 GUV. (B) Deformation profile of 2% and 4% w/v PEG 800 GUVs, n = 3. Shaded rectangular box denotes approximate duration of electric field application. Shaded areas in the traces in indicate ± SD. (C) Comparison and statistical analysis of maximum GUV deformation of each GUV conditions indicated. Note that max a/b ratio of 8% was 1 for all vesicles analyzed and thus has no error bars. Data represent mean maximum deformation and error bars denote ± SE. $N_{2\%}$ = 13, $N_{4\%}$ = 11, and $N_{8\%}$ = 12. Scale bars, 10 μm.

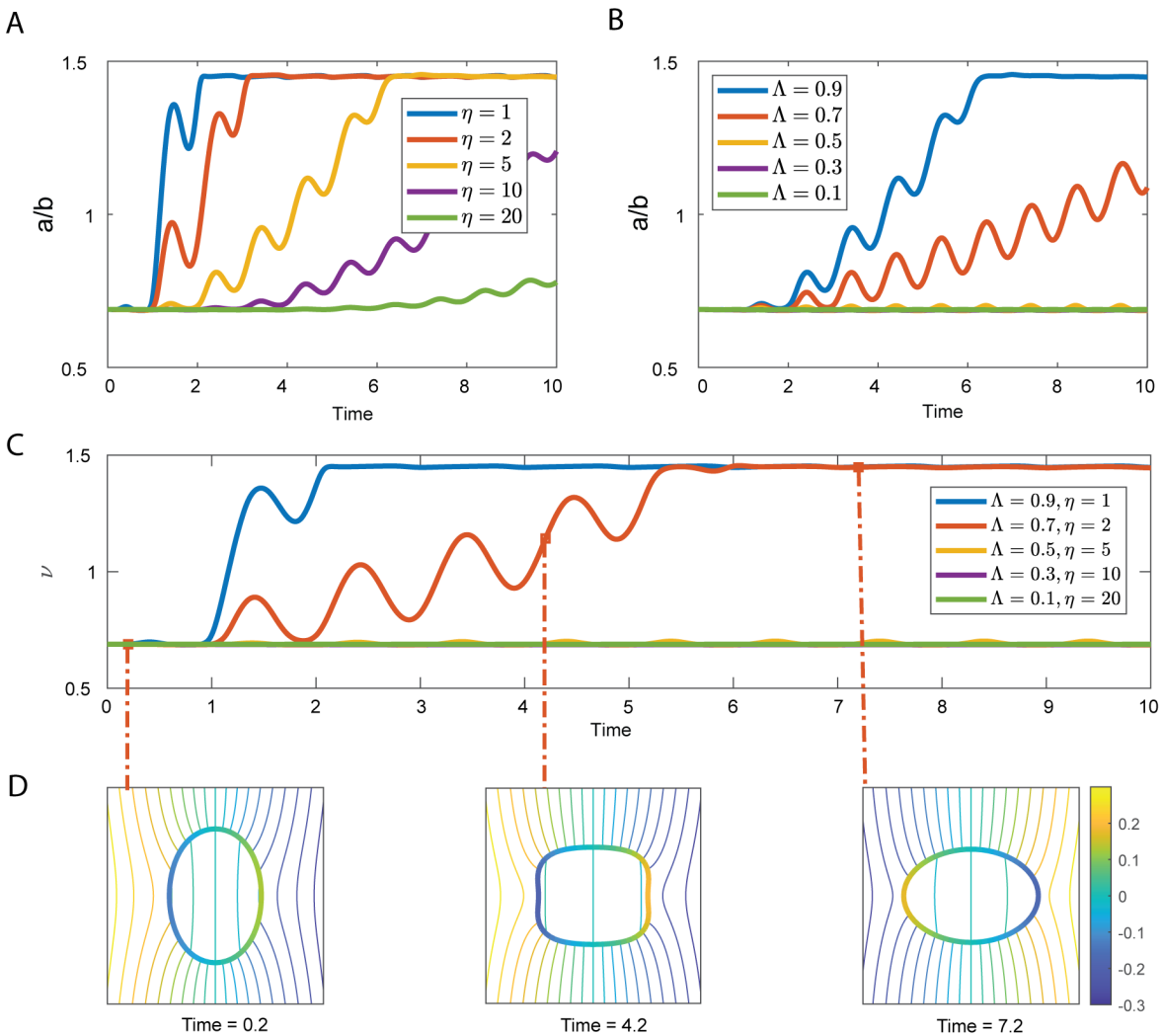


Figure 4. Prolate deformation of a GUV suspended in an AC field (β = 10, Ω = 0.5) obtained via numerical simulations. (A) Electrodeformation for various viscosity contrasts η while the conductivity ratio is fixed (Λ = 0.9). We observe that the higher GUV luminal viscosity, the longer the time it takes to complete the prolate deformation. (B) Conductivity ratio is varied while the viscosity contrast is fixed to η = 5. Prolate deformation takes longer as Λ is reduced and halts altogether below a threshold Λ . (C) Decreasing Λ and increasing η simultaneously results in a compounding effect on the prolate deformation, which is highlighted in this experiment. (D) Electric potential contour plots around the vesicle of Λ = 0.7, η = 2 at times t = 0.2 (flaccid GUV) t = 4.2 (transitionary phase) and t = 7.2 (prolate).

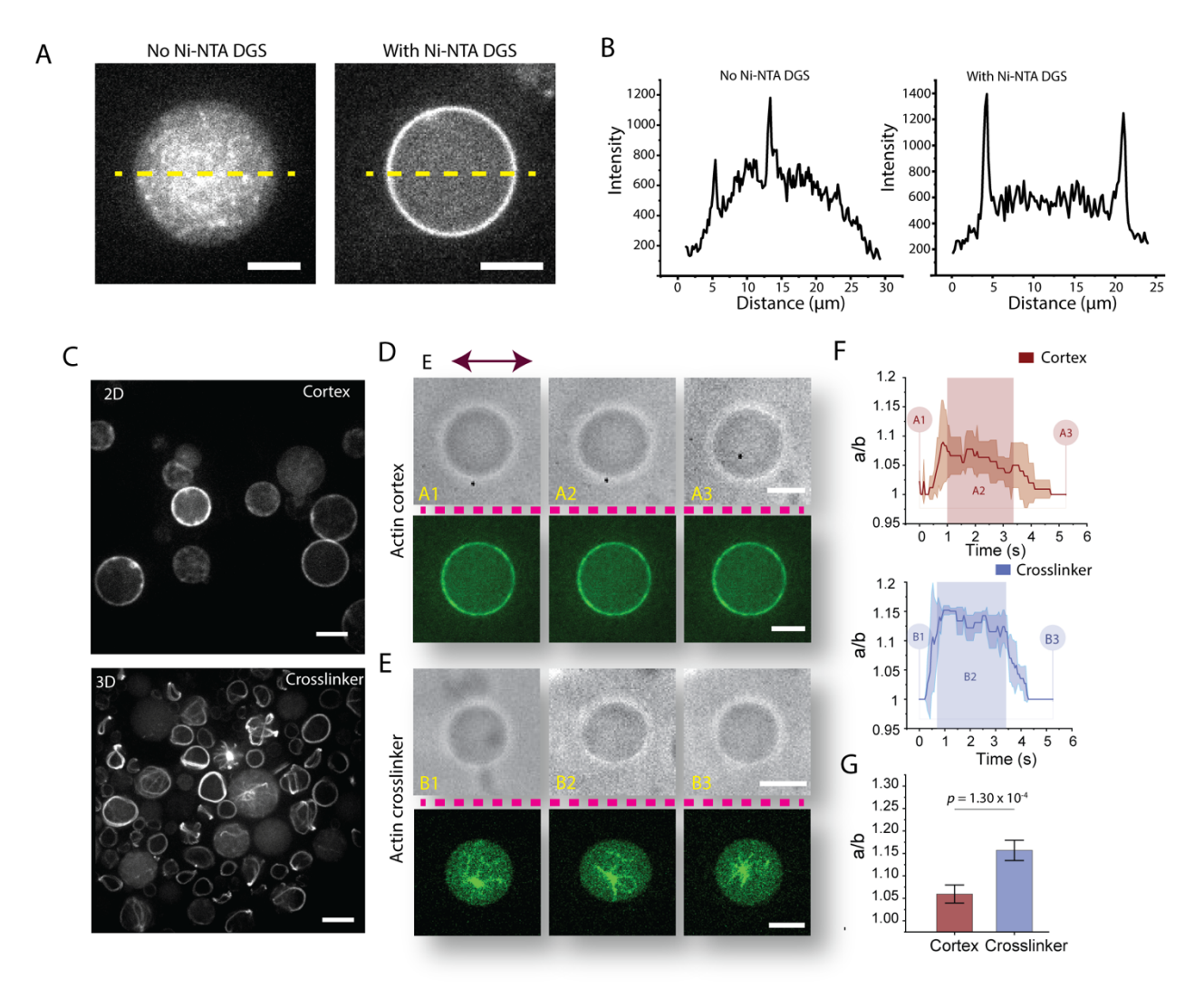


Figure 5. Actin networks reduce deformation induced by AC field electroperturbation. (A) Comparison of actin-cortex reconstitution with and without 5% Ni-NTA DGS. (B) Plots of GUV intensity profile of across the dashed line in (A). (C) High efficiency reconstitution of actin-cortex GUVs and alpha-actinin-crosslink GUVs using the modified cDICE method. (Top) Representative confocal image of Arp2/3 complex-assembled dendritic-actin-cortex GUVs. GUVs have a uniform actin cortex shell associated to the membrane via His₀-tag-nickel interaction. (Bottom) Representative confocal image of alpha-actinin-crosslink GUVs. Various actin network phenotypes commonly seen with actin networks with large-angle crosslinkers were observed. Both images show ATTO 488 actin labeling actin networks. (D) Electroperturbation of actin-cortex GUV. (Top) Brightfield images showing shape transitions pre (A1), during (A2) and post (A3) application of AC electric field. (Bottom) Confocal images of ATTO 488 actin showing actin cortex GUVs corresponding to A1, A2, and A3, (E) Electroperturbation of alpha-actinin-crosslink GUV. (Top) Brightfield images showing shape transitions pre (B1), during (B2) and post (B3) application of AC electric field. (Bottom) Confocal images of ATTO 488 actin showing alpha-actinin-crosslink GUVs at different stages of electroperturbation. Images in D) and E) separated by dotted lines are not from the same vesicles. (F) Deformation profile of actin-cortex GUVs (Top) and alpha-actinin-crosslink GUVs (Bottom) GUVs. n = 3. Shaded rectangular box denotes approximate duration of electric field

application. Shaded areas in the traces in indicate \pm SD. (G) Statistical analysis of electrodeformed actin-cortex and alpha-actinin-crosslink GUVs. Data represent mean maximum deformation and error bars denote \pm SE. N_{cortex} = 12 and $N_{crosslinker}$ = 11. Scale bars, 10 μ m.

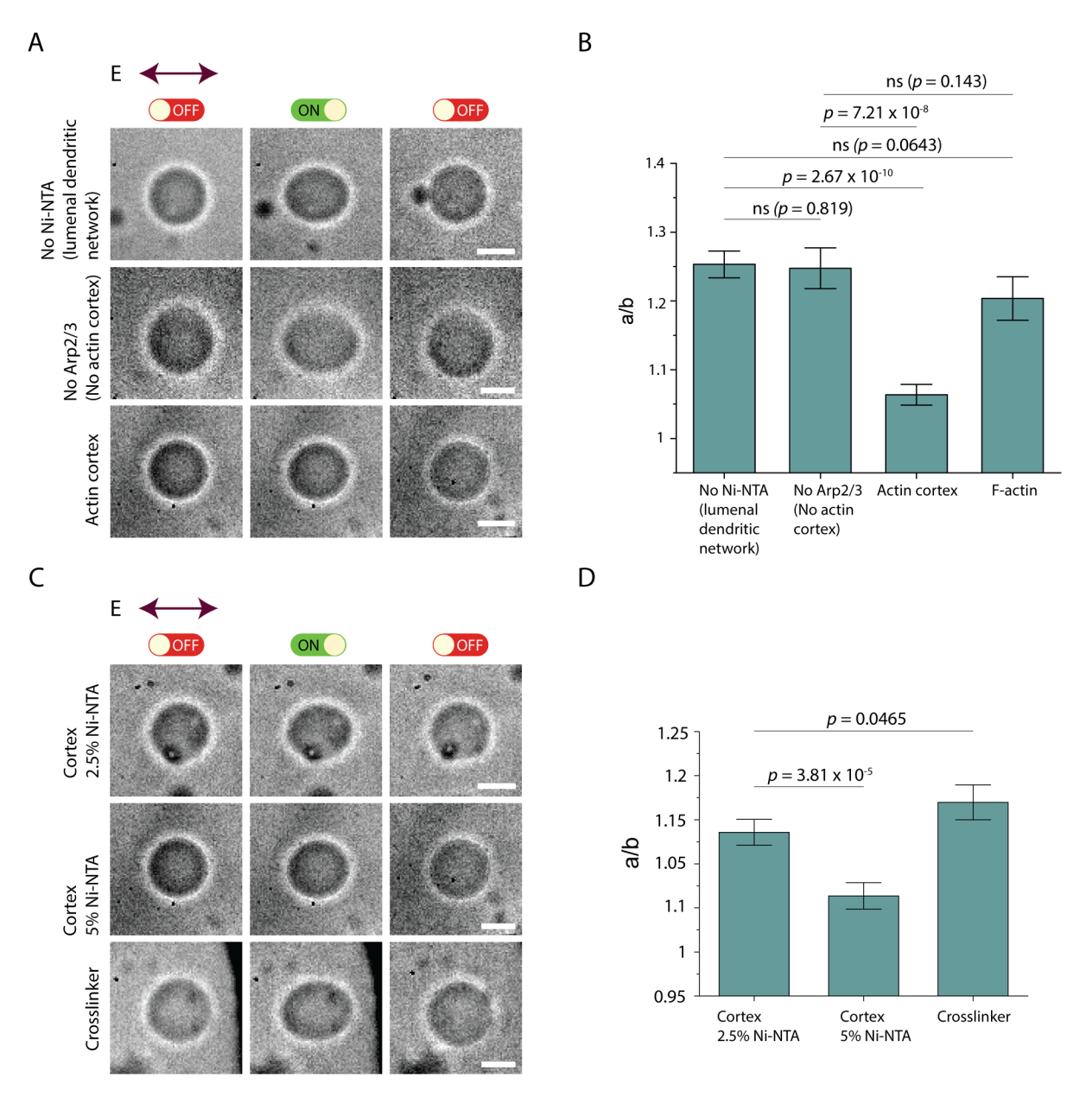


Fig. 6. Electrodeformation of GUVs encapsulating different membrane and actin binding protein conditions. (A) Brightfield images show transformation of GUVs from unperturbed (left column) to elliptically electrodeformed during application of electric field (middle column) to spherical recovery (right column). Images of GUV encapsulating 5.6 μM actin, VCA (0.5 μM), and Arp2/3 (0.5 μM) without Ni-NTA at the membrane (1st row), GUV encapsulating actin VCA excluding Arp2/3 with 5% Ni-NTA at the membrane (2nd row), actin-cortex GUV (3rd row). (B) Maximum a/b ratio of GUVs from the three conditions indicated. (C) Electrodeformation of actin-cortex at varying Ni-NTA concentrations in lipid bilayer membrane and alpha-actinin-crosslinked GUVs. Brightfield images show transformation of GUVs from unperturbed (left column) to elliptically electrodeformed during application of electric field (middle column) to spherical recovery (right column). Images of actin-cortex GUVs reconstituted in 2.5% Ni-NTA (top), 5% Ni-NTA (middle),

and alpha-actinin-crosslinked (1.77 μ M) GUVs are displayed. (D) Maximum a/b ratio of GUVs from the three conditions indicated. For (B), data represent mean maximum deformation and error bars denote \pm SE. N_{2.5% Ni-NTA} = 11, N_{5% Ni-NTA} = 13, N_{crosslinker} = 12. For (D), data represent mean maximum deformation and error bars denote \pm SE. N_{No Ni-NTA} = 10, N_{No Arp2/3} = 12, N_{Cortex} = 12, N_{F-actin} = 13. Scale bars, 10 μ m.